

pH-Controlled Assembly of 3D and 2D Zinc-Based Metal-Organic Frameworks with Tetrazole Ligands

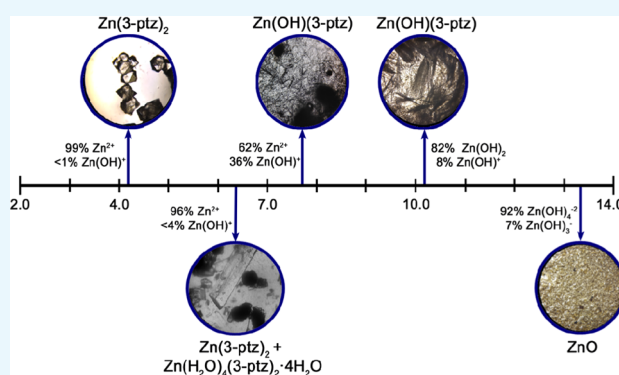
Ignacio Chi-Durán,[†] Javier Enriquez,[†] Carolina Manquian,[†] Kerry Wrighton-Araneda,[‡] Walter Cañon-Mancisidor,^{‡,§} Diego Venegas-Yazigi,^{‡,§} Felipe Herrera,^{*,†} and Dinesh Pratap Singh^{*,†}

[†]Department of Physics, Universidad de Santiago de Chile, Avenida Ecuador 3493, Estación Central, 9170124 Santiago, Chile

[‡]Departamento de Química de los Materiales, Facultad de Química y Biología, Avenida Libertador Bernardo O'Higgins 3363, Estación Central, 9170022 Santiago, Chile

[§]Center for the Development of the Nanoscience and Nanotechnology CEDENNA, Avenida Libertador Bernardo O'Higgins 3363, Estación Central, 9170022 Santiago, Chile

ABSTRACT: We report the synthesis and structural diversity of Zn(II) metal-organic framework (MOF) with in situ formation of tetrazole ligand 3-ptz [3-ptz = 5-(3-pyridyl)tetrazolate] as a function pH. By varying the initial reaction pH, we obtain high-quality crystals of the noncentrosymmetric three-dimensional MOF $\text{Zn}(\text{3-ptz})_2$, mixed phases involving the zinc-aqua complex $[\text{Zn}(\text{H}_2\text{O})_4(\text{3-ptz})_2] \cdot 4\text{H}_2\text{O}$, and two-dimensional MOF crystals $\text{Zn}(\text{OH})(\text{3-ptz})$ with a tunable microrod morphology, keeping reaction time, temperature, and metal–ligand molar ratio constant. Structures are characterized by X-ray diffraction, scanning electron microscopy, Fourier transform infrared spectroscopy, and UV–vis spectroscopy. We discuss the observed structural diversity in terms of the relative abundance of hydroxo-zinc species in solution for different values of pH.



INTRODUCTION

Metal-organic frameworks (MOFs), a novel class of functional crystalline materials,¹ have found a wide range of applications due to their favorable properties for gas storage and separation,² sensing,³ energy storage,⁴ light harvesting,⁵ drug delivery,⁶ and nonlinear optics.⁷ Depending on the choice of organic ligands, metal nodes, and synthesis conditions, self-assembled MOF structures can have a rich variety of topologies and dimensionalities.⁸ Predicting the equilibrium MOF structures obtained by solvothermal synthesis⁹ is in general challenging due to the multiple parameters that determine the self-assembly process, such as metal–ligand molar ratio,¹⁰ reaction time and temperature,¹¹ solvent polarity,¹² and reaction pH.¹³ However, it is possible to activate or deactivate specific coordination modes of multidentate ligands by controlling the reaction pH, which is a robust and cost-effective way to manipulate the MOF self-assembly process.

Tetrazole-based ligands have attracted much attention in coordination chemistry due to their large number of coordination modes involving up to four nitrogen atoms,¹⁴ which can result in a large combination of possible MOF structures with different topologies and dimensionality. Tetrazole derivatives have also excellent linear and nonlinear optical properties. For example, push–pull tetrazole complexes with both electron-donor and electron-acceptor substituents have shown very efficient second-order nonlinear optical activity in powder

samples,¹⁵ ferroelectric behavior,¹⁶ and strong photoluminescence.¹⁷

Under hydrothermal conditions, pyridyl-tetrazoles ligands exhibit six coordination modes and the pyridyl moiety can further coordinate to additional metal ions, giving rise to a potentially large number of MOF structures.^{15c,d,18} Despite the multiple coordination modes available for pyridyl-tetrazole ligands, only nine MOF structures with zinc salts have been reported via in situ ligand synthesis.^{15c,d,19} One possible route to direct the self-assembly of MOF structures is by controlling the reaction pH, which in turn controls the relative abundance of distinct metal-ion species in solution. The relative abundance of hydroxo-zinc species at different pHs can promote certain MOF structures over others, by changing the available coordination modes of the metal ion, for fixed metal–ligand molar ratio and hydrothermal conditions.

In this work, we use the initial reaction pH as a control variable to drive the synthesis of different types of zinc-based metal-organic frameworks and mononuclear complexes with in situ formation of pyridyl-tetrazole ligands, as well as zinc oxide. We discuss the crystal structure and morphology of the obtained materials and interpret the observed structural diversity in terms

Received: November 14, 2017

Accepted: January 5, 2018

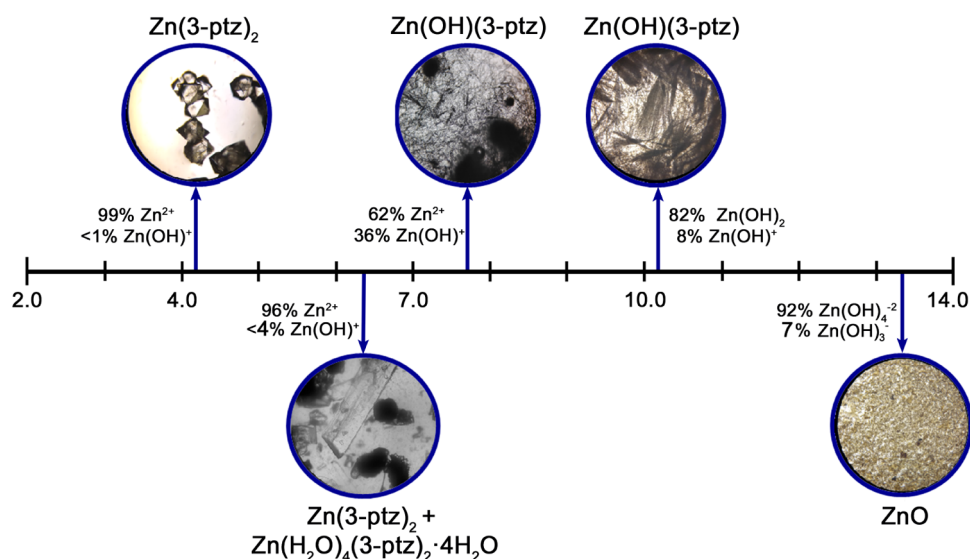


Figure 1. Microscope images of the materials obtained at different initial pH values, together with the relative abundance of hydroxy-zinc majority species in aqueous solution at 25 °C.²⁰ Acidic environments result in either pure tetrahedral crystals $\text{Zn}(\text{3-ptz})_2$ (3D MOF) or a mixed phase with zinc-tetra-aqua complex $\text{Zn}(\text{H}_2\text{O})_4(\text{3-ptz})_2 \cdot 4\text{H}_2\text{O}$ (ZAC). Basic environments result in elongated crystals of $\text{Zn}(\text{OH})(\text{3-ptz})$ (2D MOF) and zinc oxide (ZnO) for the highest pH values.

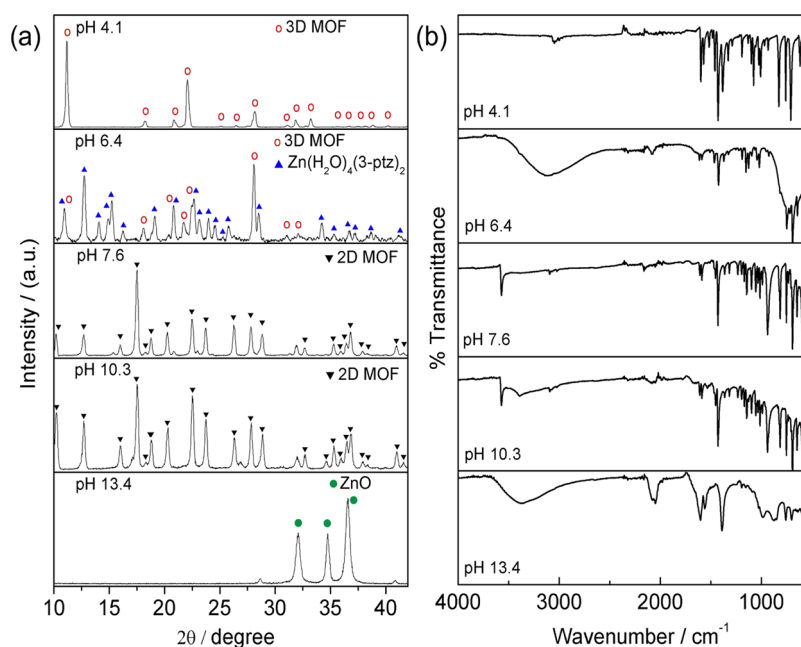


Figure 2. Structural analysis of the obtained materials as a function of pH. (a) X-ray powder diffraction patterns for five samples obtained at different initial pH values. Diffraction peaks are labeled according to the simulated pattern for $\text{Zn}(\text{3-ptz})_2$ (3D MOF), $\text{Zn}(\text{H}_2\text{O})_4(\text{3-ptz})_2 \cdot 4\text{H}_2\text{O}$ (ZAC), $\text{Zn}(\text{OH})(\text{3-ptz})$ (2D MOF), and zinc oxide (ZnO). (b) Fourier transform infrared spectra for the same samples in (a).

72 of the relative abundance of different zinc species in solution as a
73 function of pH.

74 ■ RESULTS AND DISCUSSION

75 **Figure 1** shows representative optical microscope images of the
76 crystals obtained at different initial pH values. For a range of low
77 pH values, we obtain highly pure crystals with a well-defined
78 tetrahedral morphology, corresponding to the three-dimensional
79 metal-organic framework (3D MOF) bis[5-(3-pyridyl)-
80 tetrazolato]zinc(II) [$\text{Zn}(\text{3-ptz})_2$], as confirmed below by X-ray
81 powder diffraction (XRD). The same $\text{Zn}(\text{3-ptz})_2$ MOF forms
82 also in the neutral pH range (pH 6.0–7.0), in addition to other

zinc-tetrazole coordination structures that we describe below. 83
For initial pH values exceeding 7.0, we obtain large quantities of 84
thin, ultralong microrod structures that we identify below as a 85
two-dimensional MOF (2D MOF). We obtain 2D MOF crystals 86
with visibly larger microrod lengths at higher pH values in the 87
range 10–12. Strongly basic environments (pH > 12) do not lead 88
to MOF formation. Instead, we obtain large quantities of ZnO 89
nanostructures.²¹ 90

Figure 2a,b shows the measured X-ray powder diffraction 91
(XRD) patterns and the Fourier transform infrared (FTIR) 92
spectra, respectively, of the materials obtained within the range of 93
pH shown in **Figure 1**. For pH values in the lower range (pH < 94

95 5.0), the diffraction peaks are in excellent agreement with the
 96 simulated XRD pattern reported for the tetragonal $\text{Zn}(\text{3-ptz})_2$
 97 structure.^{15c} For pH values slightly below 7.0, we obtained mixed
 98 phases of the 3D MOF $\text{Zn}(\text{3-ptz})_2$ and the triclinic crystal
 99 $\text{Zn}(\text{H}_2\text{O})_4(\text{3-ptz})_2 \cdot 4\text{H}_2\text{O}$ (ZAC).²²

100 In general, for the formation of zinc-based MOFs with in situ
 101 formation of 3-ptz ligands, the pH of the reaction must allow zinc
 102 species in solution to act as Lewis acid catalyzers of the reaction
 103 that forms 3-ptz from sodium azide and cyanopyridine.^{19c,23} The
 104 catalyzing character of the solvated metal complexes that form in
 105 our system is only inhibited under highly basic conditions. From
 106 the relative abundance of dissolved zinc hydroxide species in
 107 water,²⁰ we expect the concentration of $\text{Zn}(\text{OH})_4^{2-}$ to grow at
 108 higher pH values, decreasing the ability of zinc(II) to catalyze the
 109 ligand formation reaction. For the range of pH values in which
 110 the zinc species $\text{Zn}^{2+}_{(\text{aq})}$, $\text{Zn}(\text{OH})^+_{(\text{aq})}$, $\text{Zn}(\text{OH})_{2(\text{aq})}$, and
 111 $\text{Zn}(\text{OH})_3^-_{(\text{aq})}$ become more abundant,²⁰ we expect the 3-ptz
 112 ligand to form in situ, due to the Lewis acid character of these
 113 zinc and zinc-hydroxo species.

114 The formation of a highly pure phase of $\text{Zn}(\text{3-ptz})_2$ crystals
 115 under acidic conditions (Figure 2a, pH 4.1) is consistent with the
 116 dominant availability of the octahedral solvated Zn^{2+} ions (strong
 117 Lewis acid) at the mixing temperature,²⁰ which favors both in situ
 118 ligand formation and the tetrahedral symmetry of the 3D MOF
 119 assembly process.^{15c} Steric effects associated with the size of the
 120 3-ptz ligands lower the symmetry of the coordination sphere
 121 from octahedral to tetrahedral as water is displaced upon MOF
 122 assembly.

123 Increasing the pH closer to the neutral range (Figure 2a, pH
 124 6.4) increases the fraction of $\text{Zn}(\text{OH})^+$ species in solution
 125 relative to Zn^{2+} ,²⁰ promoting the formation of ZAC in a mixed
 126 phase with $\text{Zn}(\text{3-ptz})_2$ under hydrothermal conditions. This
 127 mixed phase can be purified by filtering the $\text{Zn}(\text{3-ptz})_2$ crystals at
 128 105 °C after completion of the reaction time. Further increasing
 129 the pH beyond the neutral range (Figure 2a, pH 7.6, 10.3) results
 130 in a highly pure crystal phase with XDR patterns that match the
 131 reported MOF catena-((μ_3 -5-(3-pyridyl)tetrazol- N,N',N'')-(μ_2 -
 132 hydroxo)-zinc [$\text{Zn}(\text{OH})(\text{3-ptz})$],^{15d} in which hydroxyl ligands
 133 along the c crystal axis bridge adjacent 2D zinc-tetrazole
 134 coordination networks on the a - b plane. Preferential growth
 135 along the c direction results in the quasi-one-dimensional (1D)
 136 rodlike morphology shown in Figure 1.

137 The formation of ZAC and 2D MOF structures in nonacidic
 138 environments can be partly understood in terms of the greater
 139 relative abundance of the solvated $\text{Zn}(\text{OH})^+_{(\text{aq})}$ and $\text{Zn}(\text{OH})_{2(\text{aq})}$
 140 species at the mixing temperature.²⁰ The strong Zn-OH
 141 coordination bond results in a solvated coordination sphere
 142 with lower symmetry than the octahedral coordination sphere of
 143 the hexa-aquo Zn^{2+} ion, which is the dominant species at lower
 144 pH. The 3-ptz ligands thus prefer to coordinate with the zinc ion
 145 in directions orthogonal to the Zn-OH bond, minimizing steric
 146 effects, a bonding pattern exhibited in both ZAC²² and 2D
 147 MOF^{15d} crystals.

148 Figure 2b shows that there are pH-dependent infrared
 149 absorption features in the region 2500–4000 cm^{-1} . For lower
 150 pH values, a weak C-H stretch band at 3048 cm^{-1} of the
 151 pyridine ring in $\text{Zn}(\text{3-ptz})_2$ is clearly visible. However, in the pH
 152 range 6.0–7.0, where the zinc-tetra-aqua complex ZAC forms,
 153 the much broader and intense O-H stretch band associated with
 154 hydrogen bonding dominates that spectral region. In the pH
 155 range 7.0–12.0, the broad O-H band disappears in favor of a
 156 much sharper O-H stretch peak (3572 cm^{-1}) associated with
 157 free hydroxyl ligands in $\text{Zn}(\text{OH})(\text{3-ptz})$. In summary, the FTIR

spectra confirm the reported bands for pyridyl-tetrazole^{15c,d} 158
 below pH 12.0. For pH above 12.0, we obtain the characteristic 159
 spectra of ZnO.^{21,24} 160

Figure 3a shows a representative scanning electron micros- 161 f
 copy (SEM) image of $\text{Zn}(\text{3-ptz})_2$ MOF crystals obtained with 162

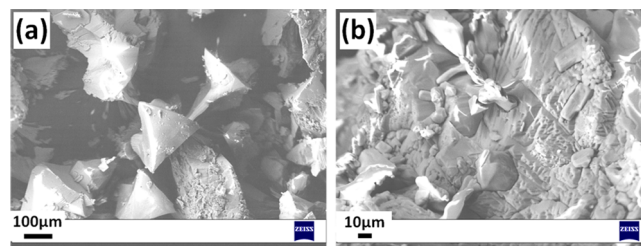


Figure 3. SEM images of sample obtained at pH 4.1 for two different magnifications.

high purity in the lower pH range, exhibiting well-defined 163
 tetragonal-shaped crystals with size varying in the range of 100– 164
 200 μm . The magnified image in Figure 3b of the same sample 165
 shows the growth of smaller nanostructures on the surface of the 166
 largest MOF crystallites. 167

Figure 4 shows representative SEM images of the material 168 f4
 obtained in the neutral pH range, featuring smaller and less- 169

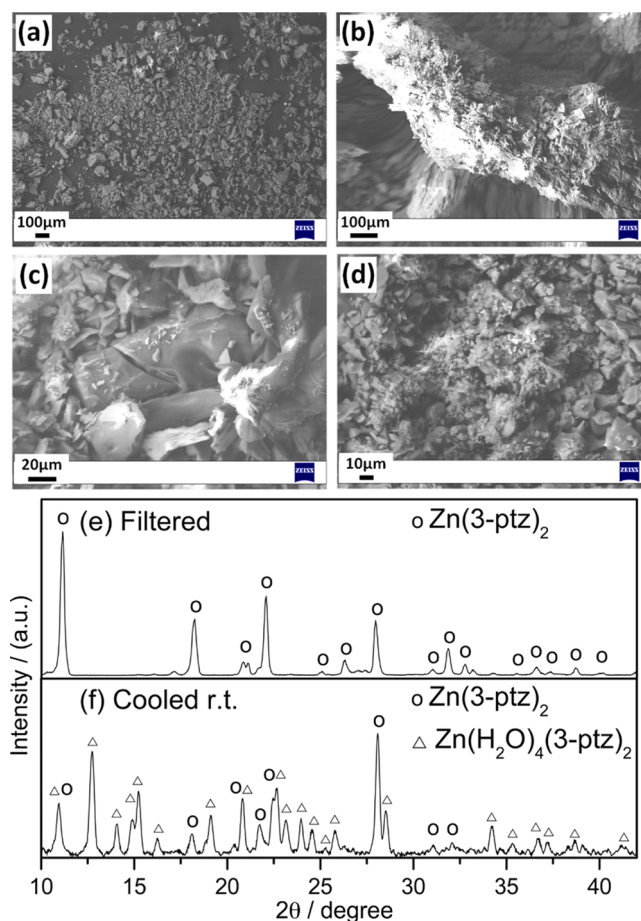


Figure 4. SEM images of sample obtained at pH 6.5. (a–d)
 Representative SEM images for different magnifications. XRD patterns
 of pH 6.47. (e) Filtered at 105 °C and (f) cooled at room temperature
 without filtering.

170 defined crystallites than those obtained at lower pH. We
 171 discussed above that this pH range gives mixed phases of $\text{Zn}(\text{3-ptz})_2$
 172 and the tetra-aqua complex ZAC. Figure 4a–d shows that
 173 the presence of tetra-aqua complex affects the superficial growth
 174 and hence the morphology of the $\text{Zn}(\text{3-ptz})_2$ MOF crystals. We
 175 find that by filtering the reaction products at 105 °C, immediately
 176 after completion of the reaction, it is possible to separate the
 177 desired 3D MOF $\text{Zn}(\text{3-ptz})_2$ from the tetra-aqua byproduct
 178 efficiently, as shown in Figure 4e,f. From the reaction yield upon
 179 filtering, we estimate that at least twice as much of zinc ions are
 180 involved in the formation of the 3D MOF crystal in comparison
 181 to the tetra-aqua complex at 105 °C. Following the reported
 182 synthetic procedure without hot filtration,^{15c} an equilibrium is
 183 established between the zinc-tetra-aqua complex and $\text{Zn}(\text{3-ptz})_2$
 184 MOF upon cooling to room temperature, giving the mixed-phase
 185 XRD pattern in Figure 4d.

186 Figure 5 shows representative SEM images of the materials
 187 obtained in basic initial environments. This pH range gives a pure

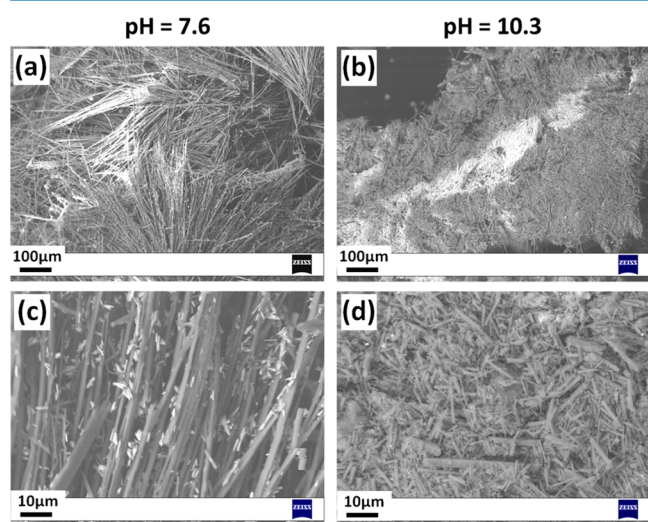


Figure 5. SEM images of as-synthesized materials in alkaline initial environments, exhibiting homogeneous microrod-type structures corresponding to $\text{Zn}(\text{OH})(\text{3-ptz})$ crystals. Different magnifications of (a, c) long microrod structures obtained at pH 7.6 and (b, d) short microrod structures obtained at pH 10.3.

188 phase of 2D MOF $\text{Zn}(\text{OH})(\text{3-ptz})$. For the most moderate
 189 alkaline initial conditions (pH 7.6), Figure 5a,c shows the growth
 190 of relatively long microrods with lengths varying in the range of
 191 300–400 μm , and widths in the range of 1.5–2.0 μm . Magnified
 192 images exhibit the growth of large quantities of comparatively
 193 smaller crystals with sizes on the order of 2 μm or less on the
 194 surface of the long microrod structures. Figure 5b,d shows that
 195 for pH 10.3 the nucleation rate is much higher, as we observe
 196 large amounts of smaller microrod 2D MOF structures with a
 197 broad length distribution in the range of 1–10 μm . The observed
 198 microrod morphology of MOF $\text{Zn}(\text{OH})(\text{3-ptz})$ is consistent
 199 with the Bravais–Friedel–Donnay–Harker (BFDH) morphol-
 200 ogy predictions shown in Figure 6. Despite the 2D coordination
 201 topology, the 1D (rodlike) morphology of the crystal results
 202 from the preferred growth in the direction orthogonal to the
 203 coordination planes. Microrods can form by preferential growth
 204 in the c direction, likely due to the self-assembly process between
 205 zinc hydroxide species coordinating to (3-ptz) ligands and
 206 hydroxyl ions, generating the $\text{Zn}-\text{OH}-\text{Zn}-\text{OH}-\text{Zn}$ chains in
 207 this direction, as reported by single-crystal diffraction.^{15d}

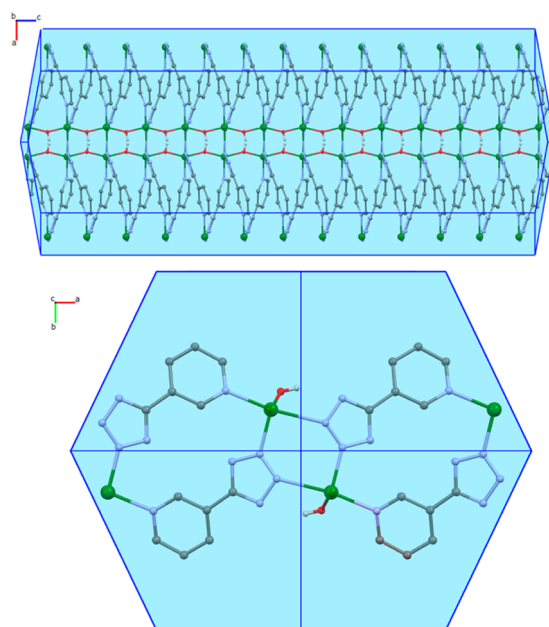


Figure 6. Morphology of 2D MOF structure $\text{Zn}(\text{OH})(\text{3-ptz})$ obtained by BFDH calculations. Zn (green), N (light blue), C (gray), O (red), and H (white).

Figure 7 shows the room-temperature solid-state UV–vis
 absorption spectra of 3D MOF $\text{Zn}(\text{3-ptz})_2$ representative of the

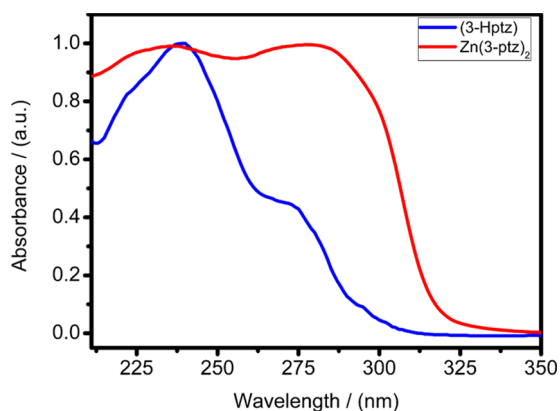


Figure 7. Room-temperature solid-state UV–vis absorption spectrum of $\text{Zn}(\text{3-ptz})_2$ MOF (red curve), featuring two strong absorption peaks at 234 and 273 nm. For comparison, the absorption spectrum of the hydrated tetrazole ligand (3-Hptz) in aqueous solution is also shown (blue curve). $\text{Zn}(\text{3-ptz})_2$ and (3-Hptz) spectra are normalized by their absorbance at 278 and 240 nm, respectively.

samples obtained in the lower pH range. The 3D MOF crystal
 does not absorb in the visible region because zinc ions in the
 framework have a closed shell (d^{10}). Density functional theory
 calculations confirm that the absorption spectrum of the
 mononuclear complex $\text{Zn}(\text{3-ptz})_2$ is dominated by $\pi-\pi^*$
 transitions in the tetrazole ligand 3-ptz. For comparison, Figure
 7 also shows the absorption spectrum of protonated pyridyl-
 tetrazole ligand 3-Hptz in aqueous solution. In the 3D MOF
 crystal, the lowest-energy π -transition is red-shifted by 9 nm
 (1194 cm^{-1}) relative to the protonated ligand spectrum and also
 becomes more intense. This behavior may indicate a possible
 electrostatic interaction between the ligand transition dipole
 moments in the solid phase.²⁵

223 ■ CONCLUSIONS AND OUTLOOK

224 We explore the structural diversity of zinc-tetrazole metal-
225 organic frameworks (MOFs) with in situ ligand formation by
226 modifying the initial pH of the reaction mixture. Optimal yield
227 and high purity of the noncentrosymmetric 3D MOF structure
228 $\text{Zn}(\text{3-ptz})_2$ ^{15c} was obtained under acidic conditions (pH \approx 4).
229 Alkaline environments strongly favor the assembly of the 2D
230 MOF structure $\text{Zn}(\text{OH})(\text{3-ptz})$ ^{15d} whose rodlike crystal
231 morphology can be manipulated by changing the initial reaction
232 pH within the range 7.5–11.0. The synthesis carried out without
233 initial pH manipulation (pH = 6.4) gives a mixed phase of the 3D
234 MOF $\text{Zn}(\text{3-ptz})_2$ and the zinc-tetra-aqua complex $[\text{Zn}(\text{3-}$
235 $\text{ptz})_2(\text{H}_2\text{O})_4]\cdot 4\text{H}_2\text{O}$,²² which can be efficiently separated by
236 high-temperature filtration. Although the solvothermal syntheses
237 of $\text{Zn}(\text{3-ptz})_2$ and $\text{Zn}(\text{OH})(\text{3-ptz})$ metal-organic frameworks
238 has been previously reported by varying the reaction time and
239 temperature,^{15c,d} we show for the first time that it is possible to
240 obtain these MOFs in high purity by simply varying the mixing
241 pH of the reactants.

242 We understand the role of pH throughout our experiments as a
243 modulator of the ligand formation reaction and MOF assembly
244 process. The observed pH-dependent structural diversity is
245 related to the relative abundance of solvated zinc-hydroxo
246 complexes of the form $[\text{Zn}(\text{OH})_n]^{2-n}$ in aqueous solution,²⁰
247 being the solvated Zn^{2+} ion the Lewis acid with the best reported
248 catalytic behavior for the in situ tetrazole ligand formation.²⁶ We
249 relate the appearance of $[\text{Zn}(\text{3-ptz})_2(\text{H}_2\text{O})_4]\cdot 4\text{H}_2\text{O}$ and
250 $\text{Zn}(\text{OH})(\text{3-ptz})$ in nonacidic environments to the presence of
251 strong Zn–OH bonds in the solvated zinc-hydroxo coordination
252 sphere, which force the 3-ptz ligands to coordinate zinc ions
253 orthogonal to the Zn–OH direction. We can expect that the
254 relative abundance of metal-hydroxo complexes in solution could
255 also be used as a strategy to explore the structural diversity of
256 other metal-organic frameworks with metal-catalyzed in situ
257 formation of tetrazole ligands.²⁷ Cadmium-based structures are
258 promising candidates to explore, given their proven potential to
259 catalyze the Demko–Sharpless ligand formation reaction.²⁸

260 In summary, our results show that manipulating the initial
261 reaction pH can be an economical route to engineer the assembly
262 of noncentrosymmetric zinc-tetrazole MOF structures, which
263 may become advantageous for future development of MOF-
264 based nonlinear crystals for applications in optical communica-
265 tion.⁷

266 ■ METHODS

267 The in situ synthesis of tetrazole ligands was done according to
268 the Demko–Sharpless method.²⁶ All of the reactants and
269 chemicals were purchased from Sigma-Aldrich and utilized
270 without any further purification. A mixture of 3-cyanopyridine (4
271 mmol), NaN_3 (6 mmol), and ZnCl_2 (2 mmol) was dissolved in 6
272 mL of distilled water. This mixture was transferred into a glass
273 bottle and then put in a box furnace at a high temperature of 105
274 °C for 24 h. The pH value was adjusted by using HNO_3 (66%) or
275 KOH (18.8 M) solutions immediately after mixing the reactants
276 (initial pH) and measured with a pH meter (pH 2700 Oakton).
277 The as-synthesized materials were taken out of the furnace after
278 24 h, filtered, and dried at room temperature prior to the
279 structural analysis. Powder X-ray diffraction analysis was done
280 using a X Shimadzu XRD 6000 diffractometer with $\text{Cu K}\alpha$ (λ =
281 1.5418 Å) radiation for structural characterization and phase
282 determination. Microstructural characterizations of the synthe-
283 sized materials were done by an optical microscope and a

scanning electron microscope (Zeiss EVO MA10). UV–vis solid
284 spectra were obtained at room temperature using a PerkinElmer
285 Lambda 1050 Wideband UV–vis–NIR spectrophotometer. IR
286 spectra ($4000\text{--}400\text{ cm}^{-1}$) of the compounds were obtained
287 using a Jasco FTIR-4600 spectrophotometer equipped with an
288 ATR PRO ONE. 289

Bravais–Friedel–Donnay–Harker (BFDH) theoretical crystal
290 morphology analyses were done with commercial software
291 (Mercury), from the cif file in ref 15d. DFT calculations of the
292 mononuclear $[\text{Zn}(\text{3-ptz})_4]^{2+}$ complex were carried out with
293 commercial software (Gaussian) using hybrid functional of
294 Perdew, Burke, and Ernzerhof (PBE0) to represent the electron
295 density. A triple- ζ basis set for H, C, N, and O atoms, including a
296 polarization function for nonhydrogen atoms, was employed. In
297 all calculations, 15 singlet excitations were considered. 298

299 ■ AUTHOR INFORMATION

Corresponding Authors

*E-mail: felipe.herrera.u@usach.cl (F.H.).

*E-mail: singh.dinesh@usach.cl (D.P.S.).

ORCID

Diego Venegas-Yazigi: 0000-0001-7816-2841

Felipe Herrera: 0000-0001-8121-1931

Notes

The authors declare no competing financial interest.

308 ■ ACKNOWLEDGMENTS

F.H. and D.P.S. were supported by Proyecto Basal USA 1555
309 Vridei 041731 and Fondecyt Regular 1151527. W.C.-M. and
310 D.V.-Y. were supported by Fondecyt Iniciación 1161255,
311 Financiamiento Basal FB0807 (CEDENNA), and the National
312 Laboratory for High Performance Computing NLHPC (ECM-
313 02), CMM, U de Chile. 314

315 ■ REFERENCES

- (1) Zhou, H.-C.; Long, J. R.; Yaghi, O. M. Introduction to Metal-
316 Organic Frameworks. *Chem. Rev.* **2012**, *112*, 673–674. 317
- (2) (a) Murray, L. J.; Dincă, M.; Long, J. R. Hydrogen storage in
318 metal-organic frameworks. *Chem. Soc. Rev.* **2009**, *38*, 1294–1314. 319
(b) Li, H.; Eddaoudi, M.; O’Keeffe, M.; Yaghi, O. M. Design and
320 synthesis of an exceptionally stable and highly porous metal-organic
321 framework. *Nature* **1999**, *402*, 276–279. (c) Rosi, N. L.; Eckert, J.;
322 Eddaoudi, M.; Vodak, D. T.; Kim, J.; O’Keeffe, M.; Yaghi, O. M.
323 Hydrogen Storage in Microporous Metal–Organic Frameworks. *Science*
324 **2003**, *300*, 1127–1129. 325
- (3) (a) Yi, F.-Y.; Chen, D.; Wu, M.-K.; Han, L.; Jiang, H.-L. Chemical
326 Sensors Based on Metal–Organic Frameworks. *ChemPlusChem* **2016**,
327 *81*, 675–690. (b) Chen, B.; Wang, L.; Zapata, F.; Qian, G.; Lobkovsky,
328 E. B. A Luminescent Microporous Metal–Organic Framework for the
329 Recognition and Sensing of Anions. *J. Am. Chem. Soc.* **2008**, *130*, 6718–
330 6719. (c) Chen, B.; Yang, Y.; Zapata, F.; Lin, G.; Qian, G.; Lobkovsky, E.
331 B. Luminescent Open Metal Sites within a Metal–Organic Framework
332 for Sensing Small Molecules. *Adv. Mater.* **2007**, *19*, 1693–1696. 333
- (4) (a) Liu, X.; Shi, C.; Zhai, C.; Cheng, M.; Liu, Q.; Wang, G. Cobalt-
334 Based Layered Metal–Organic Framework as an Ultrahigh Capacity
335 Supercapacitor Electrode Material. *ACS Appl. Mater. Interfaces* **2016**, *8*,
336 4585–4591. (b) Cao, F.; Zhao, M.; Yu, Y.; Chen, B.; Huang, Y.; Yang, J.;
337 Cao, X.; Lu, Q.; Zhang, X.; Zhang, Z.; Tan, C.; Zhang, H. Synthesis of
338 Two-Dimensional $\text{CoS}_{1.097}$ /Nitrogen-Doped Carbon Nanocomposites
339 Using Metal–Organic Framework Nanosheets as Precursors for
340 Supercapacitor Application. *J. Am. Chem. Soc.* **2016**, *138*, 6924–6927. 341
(c) Sheberla, D.; Bachman, J. C.; Elias, J. S.; Sun, C.-J.; Shao-Horn, Y.;
342 Dincă, M. Conductive MOF electrodes for stable supercapacitors with
343 high areal capacitance. *Nat. Mater.* **2017**, *16*, 220–224. 344

- (5) (a) Wang, J.-L.; Wang, C.; Lin, W. Metal–Organic Frameworks for Light Harvesting and Photocatalysis. *ACS Catal.* **2012**, *2*, 2630–2640. (b) Lee, C. Y.; Farha, O. K.; Hong, B. J.; Sarjeant, A. A.; Nguyen, S. T.; Hupp, J. T. Light-Harvesting Metal–Organic Frameworks (MOFs): Efficient Strut-to-Strut Energy Transfer in Bodipy and Porphyrin-Based MOFs. *J. Am. Chem. Soc.* **2011**, *133*, 15858–15861.
- (6) (a) Zheng, H.; Zhang, Y.; Liu, L.; Wan, W.; Guo, P.; Nyström, A. M.; Zou, X. One-pot Synthesis of Metal–Organic Frameworks with Encapsulated Target Molecules and Their Applications for Controlled Drug Delivery. *J. Am. Chem. Soc.* **2016**, *138*, 962–968. (b) Zhuang, J.; Kuo, C.-H.; Chou, L.-Y.; Liu, D.-Y.; Weerapana, E.; Tsung, C.-K. Optimized Metal–Organic-Framework Nanospheres for Drug Delivery: Evaluation of Small-Molecule Encapsulation. *ACS Nano* **2014**, *8*, 2812–2819. (c) Horcajada, P.; Gref, R.; Baati, T.; Allan, P. K.; Maurin, G.; Couvreur, P.; Férey, G.; Morris, R. E.; Serre, C. Metal–Organic Frameworks in Biomedicine. *Chem. Rev.* **2012**, *112*, 1232–1268.
- (7) (a) Mingabudinova, L. R.; Vinogradov, V. V.; Milichko, V. A.; Hey-Hawkins, E.; Vinogradov, A. V. Metal–organic frameworks as competitive materials for non-linear optics. *Chem. Soc. Rev.* **2016**, *45*, 5408–5431. (b) Wang, C.; Zhang, T.; Lin, W. Rational Synthesis of Noncentrosymmetric Metal–Organic Frameworks for Second-Order Nonlinear Optics. *Chem. Rev.* **2012**, *112*, 1084–1104.
- (8) McGillivray, L. R., Ed. *Metal-Organic Framework-Design and Applications*; John Wiley & Sons, 2010; pp 1–2.
- (9) Farha, O. K.; Hupp, J. T. Rational Design, Synthesis, Purification, and Activation of Metal–Organic Framework Materials. *Acc. Chem. Res.* **2010**, *43*, 1166–1175.
- (10) (a) Lü, X.-Q.; Jiang, J.-J.; Chen, C.-L.; Kang, B.-S.; Su, C.-Y. 3D Coordination Polymers with Nitrilotriacetic and 4,4'-Bipyridyl Mixed Ligands: Structural Variation Based on Dinuclear or Tetranuclear Subunits Assisted by Na–O and/or O–H...O Interactions. *Inorg. Chem.* **2005**, *44*, 4515–4521. (b) Cheng, Y.; Xu, P.; Ding, Y.-B.; Yin, Y.-G. Stoichiometry-dominated in situ formation of iodocuprate clusters and dimethyl-2,2[prime or minute]-biimidazoles as building units of coordination architectures. *CrystEngComm* **2011**, *13*, 2644–2648. (c) Liu, Y.; Qi, Y.; Su, Y.-H.; Zhao, F.-H.; Che, Y.-X.; Zheng, J.-M. Five novel cobalt coordination polymers: effect of metal–ligand ratio and structure characteristics of flexible bis(imidazole) ligands. *CrystEngComm* **2010**, *12*, 3283–3290. (d) Gao, Q.; Xie, Y.-B.; Li, J.-R.; Yuan, D.-Q.; Yakovenko, A. A.; Sun, J.-H.; Zhou, H.-C. Tuning the Formations of Metal–Organic Frameworks by Modification of Ratio of Reactant, Acidity of Reaction System, and Use of a Secondary Ligand. *Cryst. Growth Des.* **2012**, *12*, 281–288.
- (11) (a) Sun, Y.-X.; Sun, W.-Y. Influence of temperature on metal–organic frameworks. *Chin. Chem. Lett.* **2014**, *25*, 823–828. (b) Liu, G.-X.; Xu, H.; Zhou, H.; Nishihara, S.; Ren, X.-M. Temperature-induced assembly of MOF polymorphs: Syntheses, structures and physical properties. *CrystEngComm* **2012**, *14*, 1856–1864. (c) Calderone, P. J.; Banerjee, D.; Plonka, A. M.; Kim, S. J.; Parise, J. B. Temperature dependent structure formation and photoluminescence studies of a series of magnesium-based coordination networks. *Inorg. Chim. Acta* **2013**, *394*, 452–458. (d) Mahata, P.; Prabhu, M.; Natarajan, S. Role of Temperature and Time in the Formation of Infinite –M–O–M– Linkages and Isolated Clusters in MOFs: A Few Illustrative Examples. *Inorg. Chem.* **2008**, *47*, 8451–8463.
- (12) (a) Li, P.-Z.; Wang, X.-J.; Li, Y.; Zhang, Q.; Tan, R. H. D.; Lim, W. Q.; Ganguly, R.; Zhao, Y. Co(II)-tricarboxylate metal–organic frameworks constructed from solvent-directed assembly for CO₂ adsorption. *Microporous Mesoporous Mater.* **2013**, *176*, 194–198. (b) Sun, F.; Zhu, G. Solvent-directed synthesis of chiral and non-centrosymmetric metal–organic frameworks based on pyridine-3,5-dicarboxylate. *Inorg. Chem. Commun.* **2013**, *38*, 115–118. (c) Liu, T.; Luo, D.; Xu, D.; Zeng, H.; Lin, Z. Solvent induced structural variation in magnesium carboxylate frameworks. *Inorg. Chem. Commun.* **2013**, *29*, 110–113.
- (13) (a) Chen, L.; Jia, H.-Y.; Hong, X.-J.; Chen, D.-H.; Zheng, Z.-P.; Jin, H.-G.; Gu, Z.-G.; Cai, Y.-P. Construction of one pH-independent 3-D pillar-layer lead-organic framework containing tetrazole-1-acetic acid. *Inorg. Chem. Commun.* **2013**, *27*, 22–25. (b) Li, S.-L.; Tan, K.; Lan, Y.-Q.; Qin, J.-S.; Li, M.-N.; Du, D.-Y.; Zang, H.-Y.; Su, Z.-M. pH-Dependent Binary Metal–Organic Compounds Assembled from Different Helical Units: Structural Variation and Supramolecular Isomers. *Cryst. Growth Des.* **2010**, *10*, 1699–1705. (c) Gabriel, C.; Perikli, M.; Raptopoulou, C. P.; Terzis, A.; Psycharis, V.; Mateescu, C.; Jakusch, T.; Kiss, T.; Bertmer, M.; Salifoglou, A. pH-Specific Hydrothermal Assembly of Binary and Ternary Pb(II)-(O,N-Carboxylic Acid) Metal Organic Framework Compounds: Correlation of Aqueous Solution Speciation with Variable Dimensionality Solid-State Lattice Architecture and Spectroscopic Signatures. *Inorg. Chem.* **2012**, *51*, 9282–9296. (d) Kan, W.-Q.; Ma, J.-F.; Liu, Y.-Y.; Wu, H.; Yang, J. pH-Dependent assembly of two octamolybdate hybrid materials: A self-threading CdSO₄-type framework and a 3D 4-connected framework. *CrystEngComm* **2011**, *13*, 7037–7043.
- (14) Zhao, H.; Qu, Z.-R.; Ye, H.-Y.; Xiong, R.-G. In situ hydrothermal synthesis of tetrazole coordination polymers with interesting physical properties. *Chem. Soc. Rev.* **2008**, *37*, 84–100.
- (15) (a) Sahara, M.; Ichioka, H.; Yano, S.; Fujimoto, F.; Ehara, M.; Wakita, K.; Sonoda, N. Optical Second-Harmonic Generation of Tetrazole Derivatives. *Jpn. J. Appl. Phys.* **1994**, *33*, 169. (b) Chen, Q.-Y.; Li, Y.; Zheng, F.-K.; Zou, W.-Q.; Wu, M.-F.; Guo, G.-C.; Wu, A.-Q.; Huang, J.-S. A 3D-diamond-like tetrazole-based Zn(II) coordination polymer: Crystal structure, nonlinear optical effect and luminescent property. *Inorg. Chem. Commun.* **2008**, *11*, 969–971. (c) Wang, L.-Z.; Qu, Z.-R.; Zhao, H.; Wang, X.-S.; Xiong, R.-G.; Xue, Z.-L. Isolation and Crystallographic Characterization of a Solid Precipitate/Intermediate in the Preparation of 5-Substituted 1H-Tetrazoles from Nitrite in Water. *Inorg. Chem.* **2003**, *42*, 3969–3971. (d) Xiong, R.-G.; Xue, X.; Zhao, H.; You, X.-Z.; Abrahams, B. F.; Xue, Z. Novel, Acentric Metal–Organic Coordination Polymers from Hydrothermal Reactions Involving In Situ Ligand Synthesis. *Angew. Chem., Int. Ed.* **2002**, *41*, 3800–3803.
- (16) Liu, D.-S.; Sui, Y.; Chen, W.-T.; Feng, P. Two New Nonlinear Optical and Ferroelectric Zn(II) Compounds Based on Nicotinic Acid and Tetrazole Derivative Ligands. *Cryst. Growth Des.* **2015**, *15*, 4020–4025.
- (17) (a) Zheng, Y.; Wang, S.-H.; Wu, S.-F.; Zheng, F.-K.; Wu, A.-Q. Tunable photoluminescence of a dual-emissive zinc(II) coordination polymer with an in-situ generated tetrazole derivative and benzenetetracarboxylate. *Inorg. Chem. Commun.* **2015**, *53*, 20–22. (b) Zhang, Q.; Chen, D.; He, X.; Huang, S.; Huang, J.; Zhou, X.; Yang, Z.; Li, J.; Li, H.; Nie, F. Structures, photoluminescence and photocatalytic properties of two novel metal–organic frameworks based on tetrazole derivatives. *CrystEngComm* **2014**, *16*, 10485–10491. (c) Giraud, M.; Andreiadis, E.; Fisyuk, A. S.; Demadrille, R.; Pécaut, J.; Imbert, D.; Mazzanti, M. Efficient Sensitization of Lanthanide Luminescence by Tetrazole-Based Polydentate Ligands. *Inorg. Chem.* **2008**, *47*, 3952–3954. (d) Shi, L.; Li, B.; Yue, S.; Fan, D. Synthesis, photophysical and oxygen-sensing properties of a novel bluish-green emission Cu(I) complex. *Sens. Actuators, B* **2009**, *137*, 386–392.
- (18) (a) Xue, X.; Wang, X.-S.; Wang, L.-Z.; Xiong, R.-G.; Abrahams, B. F.; You, X.-Z.; Xue, Z.-L.; Che, C.-M. Hydrothermal Preparation of Novel Cd(II) Coordination Polymers Employing 5-(4-Pyridyl)-tetrazolate as a Bridging Ligand. *Inorg. Chem.* **2002**, *41*, 6544–6546. (b) Wang, X.-S.; Tang, Y.-Z.; Xiong, R.-G. Indirectly In-Situ hydrothermal preparation of a novel Ag tetrazole coordination polymer. *Chin. J. Inorg. Chem.* **2005**, *21*, 1025.
- (19) (a) Yang, W.; Lin, X.; Blake, A. J.; Wilson, C.; Hubberstey, P.; Champness, N. R.; Schröder, M. In situ synthesis of 5-substituted-tetrazoles and metallosupramolecular co-ordination polymers. *CrystEngComm* **2009**, *11*, 67–81. (b) Yang, Y.-T.; Zhao, F.-H.; Che, Y.-X.; Zheng, J.-M. Syntheses and characterization of two metal–organic frameworks with in situ-generated 5-(4-pyridyl)tetrazolate and azide. *Inorg. Chem. Commun.* **2011**, *14*, 1855–1859. (c) Ye, Q.; Li, Y.-H.; Song, Y.-M.; Huang, X.-F.; Xiong, R.-G.; Xue, Z. A Second-Order Nonlinear Optical Material Prepared through In Situ Hydrothermal Ligand Synthesis. *Inorg. Chem.* **2005**, *44*, 3618–3625.
- (20) Reichle, R. A.; McCurdy, K. G.; Hepler, L. G. Zinc Hydroxide: Solubility Product and Hydroxy-complex Stability Constants from 12.5–75 °C. *Can. J. Chem.* **1975**, *53*, 3841–3845.

- 483 (21) Anžlovar, A.; Orel, Z. C.; Kogej, K.; Žigon, M. Polyol-Mediated
484 Synthesis of Zinc Oxide Nanorods and Nanocomposites with
485 Poly(methyl methacrylate). *J. Nanomater.* **2012**, 2012, No. 760872.
- 486 (22) Mu, Y.-Q.; Zhao, J.; Li, C. Tetraaquabis[5-(3-pyridyl)tetrazolido-
487 κ N(5)]zinc(II) tetrahydrate. *Acta Crystallogr., Sect. E: Struct. Rep. Online*
488 **2010**, 66, m1667.
- 489 (23) (a) Wang, X.-S.; Tang, Y.-Z.; Huang, X.-F.; Qu, Z.-R.; Che, C.-M.;
490 Chan, P. W. H.; Xiong, R.-G. Syntheses, Crystal Structures, and
491 Luminescent Properties of Three Novel Zinc Coordination Polymers
492 with Tetrazolyl Ligands. *Inorg. Chem.* **2005**, 44, 5278–5285. (b) Zhao,
493 H.; Ye, Q.; Wu, Q.; Song, Y.-M.; Liu, Y.-J.; Xiong, R.-G. A Novel One-
494 Dimensional Zinc Coordination Polymer, [Zinc{(4,5-ditetrazoyl)-
495 imidazole}{(1,10)-phenanthroline}(H₂O)]_n. *Z. Anorg. Allg. Chem.*
496 **2004**, 630, 1367–1370. (c) Huang, X.-F.; Song, Y.-M.; Wu, Q.; Ye,
497 Q.; Chen, X.-B.; Xiong, R.-G.; You, X.-Z. 1D sodium ditetrazole
498 coordination polymer obtained through in situ hydrothermal ligand
499 synthesis. *Inorg. Chem. Commun.* **2005**, 8, 58–60.
- 500 (24) Rao, N. S.; Rao, M. V. B. Structural and Optical Investigation of
501 ZnO Nanopowders Synthesized from Zinc Chloride and Zinc Nitrate.
502 *Am. J. Mater. Sci.* **2015**, 5, 66–68.
- 503 (25) Spano, F. C. The Spectral Signatures of Frenkel Polarons in H-
504 and J-Aggregates. *Acc. Chem. Res.* **2010**, 43, 429–439.
- 505 (26) Demko, Z. P.; Sharpless, K. B. Preparation of 5-Substituted 1H-
506 Tetrazoles from Nitriles in Water. *J. Org. Chem.* **2001**, 66, 7945–7950.
- 507 (27) (a) Himo, F.; Demko, Z. P.; Noodleman, L. Density Functional
508 Theory Study of the Intramolecular [2 + 3] Cycloaddition of Azide to
509 Nitriles. *J. Org. Chem.* **2003**, 68, 9076–9080. (b) Himo, F.; Demko, Z.
510 P.; Noodleman, L.; Sharpless, K. B. Mechanisms of Tetrazole Formation
511 by Addition of Azide to Nitriles. *J. Am. Chem. Soc.* **2002**, 124, 12210–
512 12216.
- 513 (28) Venkateshwarlu, G.; Premalatha, A.; Rajanna, K. C.; Saiprakash, P.
514 K. Cadmium Chloride as an Efficient Catalyst for Neat Synthesis of 5-
515 Substituted 1H-Tetrazoles. *Synth. Commun.* **2009**, 39, 4479–4485.